Crystal Structure of the Chlamydomonas Starch Debranching Enzyme Isoamylase ISA1 Reveals Insights into the Mechanism of Branch Trimming and Complex Assembly.

Lyann Sim, Sophie R Beeren, Justin Findinier, David Dauvillée, Steven G Ball, Anette Henriksen, Monica M Palcic

▶ **To cite this version:**

Lyann Sim, Sophie R Beeren, Justin Findinier, David Dauvillée, Steven G Ball, et al.. Crystal Structure of the Chlamydomonas Starch Debranching Enzyme Isoamylase ISA1 Reveals Insights into the Mechanism of Branch Trimming and Complex Assembly.. Journal of Biological Chemistry, 2014, 289 (33), pp.22991-3003. ⟨10.1074/jbc.M114.565044⟩. ⟨hal-01059377⟩

HAL Id: hal-01059377

https://hal.science/hal-01059377v1

Submitted on 17 May 2024

HAL is a multi-disciplinary open access archive for the deposit and dissemination of scientific research documents, whether they are published or not. The documents may come from teaching and research institutions in France or abroad, or from public or private research centers.

L'archive ouverte pluridisciplinaire **HAL**, est destinée au dépôt et à la diffusion de documents scientifiques de niveau recherche, publiés ou non, émanant des établissements d'enseignement et de recherche français ou étrangers, des laboratoires publics ou privés.

HAL Authorization

THE JOURNAL OF BIOLOGICAL CHEMISTRY VOL. 289, NO. 33, pp. 22991–23003, August 15, 2014
© 2014 by The American Society for Biochemistry and Molecular Biology, Inc. Published in the U.S.A.

Crystal Structure of the *Chlamydomonas* Starch Debranching Enzyme Isoamylase ISA1 Reveals Insights into the Mechanism of Branch Trimming and Complex Assembly*

Received for publication, March 12, 2014, and in revised form, June 16, 2014 Published, JBC Papers in Press, July 3, 2014, DOI 10.1074/jbc.M114.565044

Lyann Sim[‡1], Sophie R. Beeren[‡], Justin Findinier[§], David Dauvillée[§], Steven G. Ball[§], Anette Henriksen[‡2], and Monica M. Palcic[‡3]

From the [‡]Carlsberg Laboratory, Gamle Carlsberg Vej 10, DK-1799 Copenhagen V, Denmark and the [§]Unité de Glycobiologie Structurale et Fonctionnelle, UMR 8576 CNRS-USTL, Bâtiment C9, Cité Scientifique, F-59655 Villeneuve d'Ascq, France

Background: The ISA1·ISA2 isoamylase complex is involved in starch synthesis.
Results: The ISA1 homodimer from the green algae *Chlamydomonas* is functional without ISA2 and its crystal structure is described.
Conclusion: The ISA1 structure reveals potential substrate recognition sites and explains its low selectivity toward tightly spaced branches.
Significance: Structural conservation with plant ISA1 suggests it may be a useful model for studying branch trimming.

The starch debranching enzymes isoamylase 1 and 2 (ISA1 and ISA2) are known to exist in a large complex and are involved in the biosynthesis and crystallization of starch. It is suggested that the function of the complex is to remove misplaced branches of growing amylopectin molecules, which would otherwise prevent the association and crystallization of adjacent linear chains. Here, we investigate the function of ISA1 and ISA2 from starch producing alga *Chlamydomonas*. Through complementation studies, we confirm that the *STA8* locus encodes for ISA2 and *sta8* mutants lack the ISA1·ISA2 heteromeric complex. However, mutants retain a functional dimeric ISA1 that is able to partly sustain starch synthesis *in vivo*. To better characterize ISA1, we have overexpressed and purified ISA1 from *Chlamydomonas reinhardtii* (CrISA1) and solved the crystal structure to 2.3 Å and in complex with maltoheptaose to 2.4 Å. Analysis of the homodimeric CrISA1 structure reveals a unique elongated structure with monomers connected end-to-end. The crystal complex reveals details about the mechanism of branch binding that explains the low activity of CrISA1 toward tightly spaced branches and reveals the presence of additional secondary surface carbohydrate binding sites.

The semi-crystalline property of starch is an important feature that enables large amounts of glucose to be packed into a tightly condensed form, either for temporary storage in the chloroplasts of leaves (transient starch) or for longer storage in the amyloplasts of cereals (storage starch). It is also a distinguishing feature that separates starch from its analogous storage molecule glycogen. Although both molecules are essentially linear α1,4-linked glucose polymers joined by α1,6-linked branch points, it is the non-uniform branching pattern in the amylopectin component of starch that allows adjacent linear chains to associate into double helices and crystallize. The discontinuous branching produces an amylopectin structure composed of alternating regions of amorphous branched layers and crystalline helical layers that totals ~9–10 nm in thickness (1–3). The enzymes involved in amylopectin synthesis include a collection of starch synthase and starch branching enzymes that work together to catalyze chain extension and branching reactions, respectively (for review refer to Refs. 4 and 5). Additionally, mutant studies in maize, rice, *Arabidopsis*, and *Chlamydomonas* revealed that debranching enzymes are involved in the crystallization of starch, although its mechanism is not very well understood (6–8). It is hypothesized that the debranching enzymes, notably the isoamylases ISA1[4] and ISA2 maintain the non-uniform branching pattern in amylopectin by trimming the misplaced branches that prevent adjacent linear chains from associating and crystallizing (4, 7, 9).

ISA1 is a family 13 glycoside hydrolase, which has activity for hydrolyzing α1,6-glucosidic linkages corresponding to branch points of growing amylopectin molecules. ISA2 is also classified in the family 13 glycoside hydrolase family, however, the putative catalytic residues are altered, rendering it enzymatically inactive. Despite its inactivity, ISA2 is evolutionarily conserved in plants, and has been suggested to play a role as a regulatory subunit for ISA1. In the cereal species such as rice and maize, one homomeric ISA1 and two heteromeric ISA1·ISA2 complexes exist (10, 11). In contrast, in *Arabidopsis* leaves and potato tubers, only a single heteromeric complex has been

This is an open access article under the CC BY license.

* This work was supported by the Carlsberg Foundation.
[1] To whom correspondence should be addressed. Dept. of Chemistry and Biology, Ryerson University, 350 Victoria St., Toronto, ON M5B 2K3, Canada. E-mail: lya.sim@gmail.com.
[2] Present address: Novo Nordisk A/S, Novo Nordisk Park, DK-2760 Måløv, Denmark.
[3] Present address: Dept. of Cellular and Molecular Medicine, University of Copenhagen, Blegdamsvej 3, 2200 Copenhagen N, Denmark.

[4] The abbreviations used are: ISA1, isoamylase 1 protein; ISA2, isoamylase 2 protein; *ISA1/ISA2*, isoamylase 1/2 gene; CrISA1, recombinant isoamylase 1 from *C. reinhardtii*; CrISA1·M7, recombinant isoamylase 1 in complex with maltoheptaose; M7, maltoheptaose; G(1–7), glucosyl moiety (1–7) of maltoheptaose; ISA2-HA, hemagglutinin-tagged isoamylase 2; AP, amylopectin; SBS, secondary binding site; DP, degree of polymerization; aa, amino acid; PDB, Protein Data Bank; UPLC, ultra performance liquid chromatography.

observed *in vivo*. The differences in the ISA1 and ISA1·ISA2 protein complex distribution in the species correlate with the results observed upon inactivation of either *ISA1* or *ISA2* genes through mutagenesis in *Arabidopsis* and cereals or upon decreasing transcript abundance by antisense RNA approaches in potato. In both potato and *Arabidopsis*, both ISA1 and ISA2 seem to be crucial to starch synthesis as elimination or decrease of expression of either subunit gene by such approaches has equal impact on starch synthesis (6, 12, 13). In the cereals, ISA1 seems to be the crucial component in starch synthesis as loss of ISA2 does decrease starch levels but not to the same degree as in *Arabidopsis* and potato (11, 14).

Chlamydomonas reinhardtii is an alga model for studying starch synthesis and it is able to synthesize either transient or storage starch, depending on growth in the presence or absence of nitrogen, respectively (15, 16). Under nitrogen starvation conditions, *Chlamydomonas* strains carrying mutations at either the *STA7* and *STA8* loci display phenotypes similar to that of the respective *ISA1* and *ISA2* mutants observed in the cereal species (7, 17). The *STA7* locus was proven to define the structural gene of the algal ISA1 subunit. However, the nature of the *STA8* locus has remained uncertain as this locus was solely defined through the phenotype consequences of its inactivation after random insertional mutagenesis. Mutation of the *STA7* locus leads to a very severe reduction of starch content and its replacement by a water-soluble polysaccharide phytoglycogen (7). Although not as severe as the *sta7* mutants, mutants of the *STA8* locus have also been described to accumulate both phytoglycogen and a reduced amount of high amylose starch (7, 17). In nitrogen-supplied medium, however, whereas the *sta7* mutants remain starchless (18), the *sta8* mutants display no reduction in starch content and phytoglycogen accumulation is strongly reduced (19). Although *STA7* has been shown to encode ISA1 (7), the molecular nature of the *STA8* locus and its relationship to the ISA2 protein has not previously been documented. However, due to the phenotypic similarity of the *sta8* mutants to the *ISA2* mutants in cereals, we have strong reason to believe that the *STA8* locus encodes for the ISA2 protein in *Chlamydomonas*.

In this study, we show in *Chlamydomonas* that the *STA8* locus encodes ISA2, that ISA2 interacts physically with ISA1, and confirm the presence of both homomeric ISA1 and heteromeric ISA1·ISA2 complexes *in vivo*. We also report the crystal structure of ISA1 from *C. reinhardtii* (CrISA1), the first of any plant or algae ISA1 complex. CrISA1 is shown to be an elongated homodimer with monomers connected end-to-end via their C-terminal domain. Moreover, through crystal complex studies with maltoheptaose, we have mapped the enzyme active site and determined the structural basis of branch binding and recognition by CrISA1. Finally, we compare CrISA1 with other plant ISA1, propose the conservation of the dimeric ISA1 structure in plants, and suggest how it may serve as framework for the assembly of ISA1·ISA2 heterocomplexes.

EXPERIMENTAL PROCEDURES

Chlamydomonas Strains and Growth—The wild-type 330 strain, and *sta8* mutant strains BafV13 (carrying the *sta8-1*::*ARG7* mutation) and BafO6 (carrying the *sta8-2*::*ARG7* mutation) were previously described by Dauvillée *et al.* (19). All experiments were carried out in continuous light (40 μE m^{-2} s^{-1}) in the presence of acetate at 24 °C in liquid cultures. Nitrogen-starved cultures were inoculated at 5×10^5 cells ml^{-1} and harvested after 5 days at a final density of 1 to 2×10^6 cells ml^{-1}. Formula for media and genetic techniques can be found in Harris (20).

TABLE 1
Complementation of the *sta8* mutant strains with *ISA2* or *ISA2-HA*

Strains	Genotype	Starch	AP	Amylose	Water-soluble polysaccharide
		μg 10−6 cells	λ_{max}	*%*	*μg 10−6 cells*
330	Wild-type	40 ± 6	552 ± 2	24 ± 6	0.12 ± 0.07
BaFV13	*sta8-1*	8 ± 3	599 ± 6	49 ± 7	1.70 ± 0.30
V13C	*sta8-1::ISA2*	31 ± 3	556 ± 4	19 ± 7	0.06 ± 0.04
V13HA	*sta8-1::ISA2-HA*	43 ± 8	554 ± 3	22 ± 5	0.18 ± 0.07
BaFO6	*sta8-2*	10 ± 2	603 ± 5	46 ± 8	1.10 ± 0.40
O6C	*sta8-2::ISA2*	36 ± 7	554 ± 4	21 ± 5	0.05 ± 0.02
O6HA	*sta8-2::ISA2-HA*	33 ± 5	553 ± 3	28 ± 3	0.21 ± 0.14

Functional Complementation of sta8 Mutant Strains with ISA2 or ISA2-HA—The plasmid containing full-length *ISA2* (pSL-Isa2) was constructed as follows. The full-length *ISA2* genomic DNA (8.7 kbp) (sequence ref Cre17.g698850 on phytozome) was amplified by PCR in two fragments using the Dynazyme™ Ext polymerase (Finnzymes, Espoo, Finland) following the supplied standard procedure for amplification. Flanking restriction sites were introduced into the 5′ end of the first 3.5-kb PCR product by using EcoRI Isa2F (GGA ATT CAT GAT ACA AGG ACA CGT CCA G) and IntIsa2–5 (GCC GAG TAC ACG TAC GTA CCC AG) primers, whereas a XbaI restriction site was introduced in the second 5-kb PCR product covering the end of the genomic DNA using IntIsa2–3 (GGT TCT GGC GGT TTG GTT GCG G) and XbaIsa2R (GTC TAG ATC AGT GCT TCC GGG CCG CCG C) primers. The full-length *ISA2* genomic sequence was then assembled from PCR products using a unique KpnI restriction site found in the gene and cloned into the pSL18 plasmid (21). This plasmid was called pSL-Isa2 and was used to transform Baf06 and BafV13 mutant strains with the glass beads method (22). Transformants were selected on plates containing 10 μg/ml of paromomycin and were called either O6C or V13C depending on the mutant strain transformed.

A hemagglutinin (HA)-tagged *ISA2* construct, pSL-Isa2::3HA, was obtained as follows. A PCR product covering the 3′ end of the gene using IntIsa2–3 and XbaIsa2NS (GTC TAG AGT GCT TCC GGG CCG CCG C) primers allowed deletion of the stop codon and introduction of a XbaI restriction site. The triple HA tag was inserted in the 3′ end XbaI site. The transformants containing pSL-Isa2::3HA were called either O6HA or V13HA depending on the mutant strain transformed. *Chlamydomonas* mutant strains and genotypes are summarized in Table 1.

Starch Characterization of Wild Type, sta8 Mutant, and Complemented Chlamydomonas Strains—Starches and water-soluble polysaccharides from 1 liter of nitrogen-starved culture were purified and characterized from three independent cultures of wild-type (330), *sta8* mutants (BafV13 and BafO6), and complemented strains (O6C, O6HA, V13C, and V13HA). A full account of starch characterization procedures including amyloglucosidase assays, starch purification on Percoll gradients,

and the wavelength of the maximal absorbance of the iodine-polysaccharide complex (λ_{max}), can be found in Delrue *et al.* (23). Briefly, 2 mg of each starch sample were subjected to CL-2B gel permeation chromatography (GE Healthcare) to separate amylopectin and amylose components. Both amylopectin (AP) and amylose fractions were then assayed by amyloglucosidase assay allowing the determination of the amylose content (amylose %). The wavelength at the maximum absorbance (λ_{max}) was monitored for the amylopectin of each strain. The starch and water-soluble polysaccharide amounts (in $\mu g/10^6$ cells), the percentage of amylose in starch, and the λ_{max} were averaged from three independent samples. Starch characteristic of the *Chlamydomonas* strains are summarized in Table 1.

Detection of Starch Modifying Activities and ISA1 Complexes on Zymograms—Crude extracts from wild-type, *sta8* mutant strains, and *ISA2* and *ISA2-HA* complemented strains were run on denaturing starch zymograms and native glycogen zymograms to allow identification of starch hydrolyzing activity and isoamylase complexes, respectively. Experimental conditions are detailed in Mouille *et al.* (7) and Dauvillée *et al.* (17), respectively. In each case, 100 μg of total protein extract were loaded on the gels.

Denaturing glycogen zymograms, treated under different conditions, were used to monitor starch phosphorylase and starch synthase activities. After the run, the gels were washed 4 × 30 min in 40 mM Tris, pH 7, and incubated in the presence of either ADP-glucose or glucose 1-phosphate to detect for starch synthase or starch phosphorylase activities, respectively. To allow the detection of phosphorylase activity in denaturing conditions, the first wash was performed in the presence of 20 mM pyridoxal phosphate.

ISA2-HA Pull-down in Crude Chlamydomonas Extract—Crude extracts of *Chlamydomonas* strains were prepared in purification buffer (10 mM Tris, pH 7, + protease inhibitor) at a protein concentration of 2 mg/ml. For HA pulldown experiments, 1 ml of crude extracts from ISA2-HA expressing strains were incubated with 80 μl of EZ view™ Red anti-HA affinity gel (Sigma) for 1 h at 4 °C. Beads were then washed extensively with purification buffer followed by purification buffer + 0.4 M NaCl. Bound proteins were eluted from the beads by boiling in 100 μl of a water, 20% (w/v) SDS, β-mercaptomethanol mixture (0.85/0.10/0.05 (v/v/v)). The supernatant obtained was analyzed on denaturing starch and glycogen containing zymograms.

Construct Design of Recombinant CrISA1—An *Escherichia coli* codon optimized gene encoding for amino acids 57–875 of *C. reinhardtii* isoamylase 1 (CrISA1) (GenBank™ accession number AAP88032.1) was obtained from GenScript (NJ). The first 56 N-terminal amino acids of CrISA1 were predicted to encode a chloroplast transit peptide by ChloroP (24) and subsequently excluded from the construct. The pET28a-CrISA1 plasmid was constructed by inserting the codon-optimized gene into the pET28a expression vector at NdeI/XhoI restriction sites in-frame with an N-terminal His_6 tag and thrombin cleavage site.

Purification of Recombinant CrISA1—BL21(DE3) *E. coli* cells transformed with pET28a-CrISA1 were grown at 37 °C until an A_{600} of 0.5 was reached. Cells were then induced with 0.4 mM isopropyl β-D-1-thiogalactopyranoside and incubated at 30 °C for 4 h. After the induction period, cells were harvested and resuspended in HisTrap binding buffer (20 mM Tris, pH 8.0, 500 mM NaCl, and 40 mM imidazole) and lysed using a Constant System cell disruptor and centrifuged at 40,000 × *g* for 30 min. The cleared lysate was loaded onto a 5-ml HisTrapFF Crude column, washed with HisTrap binding buffer until baseline absorbance was reached, and then eluted using an imidazole gradient. After checking purity on an SDS gel, fractions were pooled and DTT was added to a final concentration of 1 mM. Samples were concentrated (using a 30-kDa MWCO spin concentrator) and loaded onto a HiLoad Sephadex 200 26/60 column equilibrated with 10 mM Tris, pH 7.5, 150 mM NaCl, and 1 mM DTT at a flow rate of 2 ml/min. CrISA1 eluted as a single peak at an elution volume corresponding to a size of ~190 kDa, as determined from molecular weight standards (Fig. 2*A*).

CrISA1 Crystallization and Maltoheptaose Soak—CrISA1 crystals were grown at 20 °C by hanging well vapor diffusion using a 1:1 volume ratio of protein (10 mg/ml) to well solution (0.2 M triammonium citrate, pH 7.0, and 14–20% PEG3350). Crystals were cryoprotected using 30% glucose (w/v) (dissolved directly in crystallization buffer), 5% glycerol before flash freezing in liquid nitrogen. Maltoheptaose (M7) soaks were achieved by incubating crystals with 50 mM M7 dissolved in crystallization buffer, which were then cryoprotected in 30% glucose, 5% glycerol, 50 mM M7.

X-ray Data Collection and Refinement—Diffraction data of the CrISA1 and M7 soaked crystals were collected at the ESRF ID23-1 and ID23-2 beamlines, respectively. Diffraction data were processed and scaled using XDS (25). Data collection statistics are summarized in Table 2. Precision-indication merging *R* factor values (R_{pim}) (26) calculated using Aimless (27), along with data completeness and $CC_{1/2}$ (28) were considered in the determination of high-resolution cutoffs used for structural refinement. The CrISA1 structure was determined by a molecular replacement method using Phaser (29) and a CHAINSAW (30) trimmed structure of glycogen debranching enzyme TreX (PDB code 2VNC) as a search model (31). Two molecules were found in the asymmetric unit, which corresponded to a solvent content of 65%. The resulting model was rebuilt using ARP/wARP (32), which traced 97% of the structure. The remaining residues were manually built using Coot (33) and refined using restrained refinement and TLS refinement (34) in REFMAC (35). The refined model was subsequently used as a starting model for refinement of the M7-soaked CrISA1 structure. After rigid body refinement and restrained refinement in REFMAC, water was added using ARP/wARP solvent and glucose units were manually built using Coot. Using link restraints generated by JLigand (36), M7 was refined as a covalently bound intermediate. Refinement statistics are summarized in Table 2. Coordinates and structure factors for the CrISA1 and M7 soaked CrISA1 structures were deposited into the Protein Data Bank (PDB) with accession codes 4J7R and 4OKD, respectively.

Activity Assay of Recombinant CrISA1—CrISA1 activity was measured using soluble potato AP (Sigma), glycogen (Oyster Type II, Sigma), β-limit dextrin (Megazyme), and pullulan (Megazyme) substrates. Substrates stock solutions of 10 mg/ml

TABLE 2
X-ray data and structure refinement statistics

Data collection statistics	CrISA	CrISA-M7
X-ray source	ESRF ID23–1	ESRF ID23–2
Wavelength (Å)	0.976	0.873
Space group	P 41 21 2	P 41 21 2
Unit cell parameters		
a, *b*, *c* (Å)	102.13, 102.13, 488.63	102.75, 102.75, 487.81
α, β, γ (°)	90, 90, 90	90, 90, 90
Resolution range	48.7–2.30	46.0–2.30
No. of unique reflections	114,033	109,429
Redundancy	7.7 (3.6)[a]	6.5 (6.1)[a]
$I/\sigma I$	11.9 (1.53)	13.3 (1.37)
Completeness (%)	97.5 (85.8)	93.0 (64.5)
R_{pim}[b] (%)	5.0 (44.7)	5.1 (75.1)
$CC_{1/2}$[c]	99.6 (59.8)	99.8 (54.2)
Refinement statistics		
Resolution (Å)	48.7–2.30	46.0–2.40
No. of used reflections	114,031	95,751
R_{cryst}/R_{free} (%)	20.2/23.5	19.2/22.7
No. molecules per asymmetric unit	2	2
No. protein atoms	12,404	12,341
No. solvent atoms	488	433
No. ligands atoms	0	268
R.m.s. deviation bond lengths (Å)	0.007	0.009
R.m.s. deviation angles (°)	1.174	1.379
B average (Å^2)		
Protein (mon A/mon B)	37.3/34.1	54.8/51.1
Ligand-active site (G7)	NA[d]	60.4/58.3[e]
Ligand-active site (GLC)	NA	69.7/NA
Ligand-SBS 1	NA	69.6/77.0
Ligand-SBS 2	NA	84.9/NA
Solvent	34.7	47.3
Ramachandran plot (%)[f]		
Favored	95.35	95.08
Outliers	0.13	0.25
PDB ID	4J7R	4OKD

[a] Values in parentheses refer to the highest resolution bin.
[b] R_{pim}, precision-indicating merging *R* factor (26).
[c] $CC_{1/2}$, percent correlation between intensities from random half-datasets (28).
[d] NA, not applicable.
[e] Ligand associated with monomer A/monomer B, respectively.
[f] Values calculated using Molprobity (52).

were prepared in 150 mM NaCl, 50 mM MES, pH 6.5, buffer and if necessary, heated to 80 °C to dissolve. For substrate activity screening, CrISA1, at a final concentration of 0.05 mg/ml, was incubated with 2 mg/ml of substrate at 30 °C for 30 min. The reaction was terminated by heat inactivation at 95 °C before measuring reducing-end equivalents. Duplicates were prepared for each reaction.

Reducing-end equivalents were determined using the bicinchoninic acid reducing sugar assay method of Nelson (37) and Somogyi (38) using maltose as a standard. The debranching reaction was carried out in 1.5-ml microcentrifuge tubes buffered in a final buffer concentration of 40 mM MES, pH 6.5, 120 mM NaCl and a final reaction volume of 50 μl.

Time Course and HPLC Analysis of CrISA1 Debranched Amylopectin—Soluble potato AP treated with CrISA1 was analyzed at various time points to measure the chain length distribution of the released branches. A 1-ml solution of 2 mg/ml of amylopectin in 50 mM MES buffer, pH 6.0, was treated with 1 μl of CrISA1 solution (25 mg/ml) at 30 °C for 4 h. Aliquots of reaction mixture (100 μl) were removed after 1, 5, 60, and 240 min and quenched with EtOH (900 μl). These samples were evaporated to dryness *in vacuo*.

The samples were then each dissolved in a mixture 1 M 2-aminobenzamide solution (100 μl) and 1 M sodium cyanoborohydride solution (100 μl) each in 30% acetic acid in DMSO. The solutions were heated to 60 °C for 4 h. At room temperature, the solutions were diluted with H_2O (1800 μl) and washed with CH_2Cl_2 (2 × 8 ml). The aqueous layers (1.4 ml) were collected and centrifuged at 10,000 rpm for 5 min, then 20-μl aliquots of each were diluted with 180 μl of a mixture of MeCN and 10 mM ammonium formate buffer, pH 4.5 (75:25). The resulting solutions were analyzed using a Waters Acquity UPLC/MS fitted with a Waters fluorescence detector operating with excitation at 330 nm and detection at 420 nm. Separation was achieved by means of a Waters Acquity UPLC BEH Glycan 1.7 μm, 2.1 × 150-mm column operating at room temperature and with an injection volume of 5 μl. Elution conditions are listed in Table 3.

TABLE 3
UPLC elution conditions for the separation of 2-aminobenzamide-labeled maltooligosaccharides

Time (min)	Flow rate	% Solvent A (10 mM NH_4CHOO buffer, pH 4.5)	% Solvent B (MeCN)
	ml/min		
0	0.2	22	78
5	0.2	22	78
30	0.2	50	50
45	0.1	65	35
48	0.1	90	10
51	0.1	22	78
55	0.2	22	78

RESULTS

CrISA1 Activity—CrISA1 activity was screened against potato AP, glycogen, β-limit dextrin, and pullulan substrates. At 2 mg/ml of substrate concentration, CrISA1 showed the highest activity against AP, β-limit dextrin, and glycogen substrates and ~10-fold lower activity against pullulan, as typical for isoamylase-type debranching enzymes (Fig. 1*A*). Hydrolysis products of AP were labeled with 2-aminobenzamide and separated by UPLC-MS. Baseline separation of chain lengths with degree of polymerization (DP) between 2 and 30 could be achieved and peak integration suggests the majority of the peaks are >DP 6 (Fig. 1*B*). Time course digests reveals that CrISA is slower at hydrolyzing branches with DP 2–5 and that there was no apparent selectivity among branches >DP 6 (Fig. 1*C*).

Overall Structure of CrISA1—The structure of CrISA1 is composed of 3 domains characteristic of family 13 glycoside hydrolase subfamily 11 members (39). These include the highly conserved catalytic $(\beta/\alpha)_8$ A-domain (aa 184–750), N-terminal β-sandwich domain (aa 76–183), and C-terminal β-sandwich domain (aa 751–875) (Fig. 2*B*). In the crystal structure, the N-terminal region, including the His tag and residues 57–77 of CrISA1, are disordered. The overall architecture of the CrISA1 monomer is very similar to that of TreX (r.m.s. deviation 1.46 Å, PDB code 2VNC), *Pseudomonas* isoamylase (r.m.s. deviation 1.54 Å, PDB code 1BF2) (40), and glycogen debranching enzyme (r.m.s. deviation 1.55 Å, PDB code 2WSK) (41). Calcium ions, observed in the TreX and isoamylase structures at non-conserved positions, were not observed in the CrISA1 structure. This is consistent with the experimental data that suggest that these ions are not required for ISA1 activity (17).

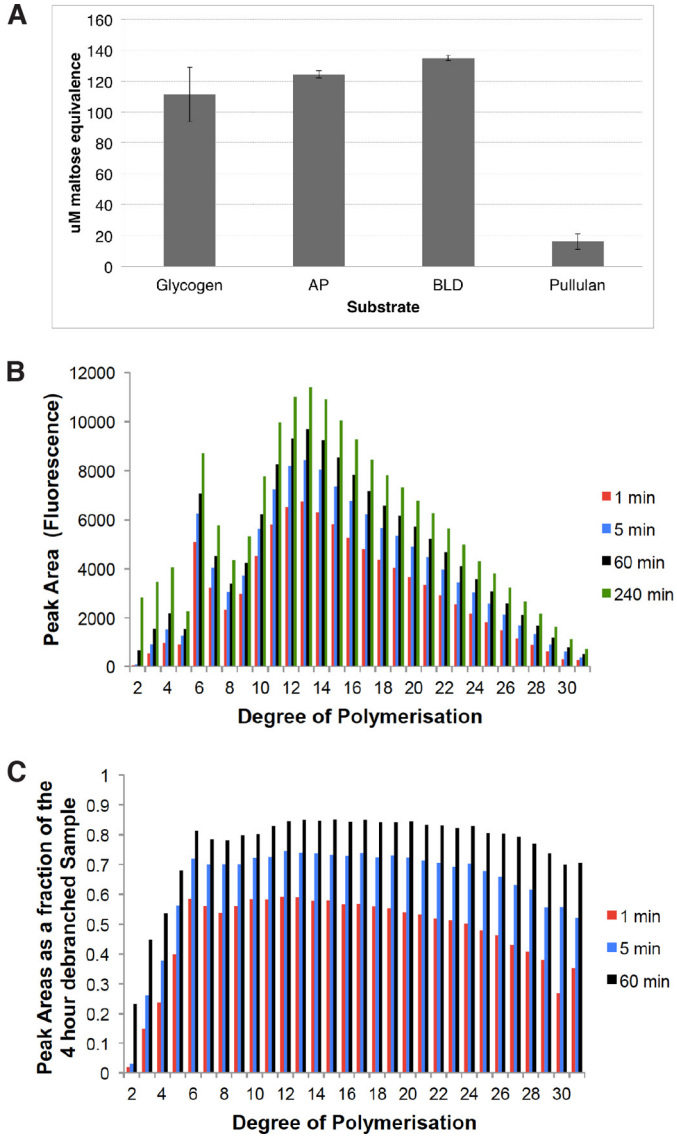

FIGURE 1. **Debranching activity of CrISA1.** *A,* substrate screen of CrISA1 activity against glycogen, amylopectin (*AP*), β-limit dextrin (*β-LD*), and pullulan substrates, each at 2 mg/ml. Activity was measured in reducing-end equivalents of maltose. *B,* profiling and quantitation of hydrolyzed AP branches at various time points as represented by peak area integration of UPLC separated and fluorescently labeled AP. *C,* relative rates of debranching as measured by fraction of the peak area from *B* at 1, 5, and 60 min compared with the peak area at 240 min.

Gel filtration chromatography indicates that CrISA1 elutes approximately at a size of 190 kDa, as estimated from molecular mass protein standards (Fig. 2*A*). As the recombinant CrISA1 is predicted to be 93.0 kDa in size and runs as a monomer on a reducing SDS-PAGE gel (Fig. 2*A*, *inset*), this suggests that under non-denaturing conditions CrISA1 assembles as a dimer. Although two monomers, A and B, exist in the asymmetric unit of the crystal structure (Fig. 2*B*), the biological dimer, assessed by the Protein interfaces, surfaces, and assemblies server (PISA) (42), is generated by monomer A and by a symmetry related copy of monomer B ($-y + 1/2, x + 1/2, z + ¼$) (Fig. 2*c*). The biological dimer is an elongated structure (~190 Å in length) with individual monomers arranged linearly in a tail-to-tail fashion via interaction with the C termini, which orients the N termini of each monomer at either end of the dimer (Fig. 2*C*). The dimerization interface is formed through the β4 and β6 strands of the C-terminal β-sandwich domain, a loop-helix element inserted between β5 and β6 and a C-terminal helix extension (Fig. 2, *D* and *E*). The 48 participating residues interact mainly via Van der Waals interactions and one salt bridge interaction between NH1 of Arg-667 and OD1 of Asp-848, resulting in a buried interface area of 1888 Å^2, representing 6.3% of the total monomer surface area. A 2-fold rotation axis, located at the center of the interface, relates the two monomers and places their active sites on the same face of the dimer (Fig. 2*C*).

Structure of CrISA1 in Complex with Maltoheptaose—The resulting structure generated from CrISA1 crystals soaked with maltoheptaose (M7) reveals significant electron density in the active site cleft of both monomers A and B (Fig. 3*a*). Following the nomenclature described by Davies *et al.* (43), the electron density spans the substrate binding groove corresponding to putative subsites −7 to −1. The glucosyl moieties of the M7 residue are numbered from the reducing to non-reducing end from G1 to G7. Moreover, connective density observed between G1 and OD1 of the catalytic nucleophile Asp-542, suggests M7 forms a covalent glycosyl intermediate with CrISA1 (Fig. 3*B*). Except for a weak density in subsite +2, interpreted as a glucose molecule from the cryoprotectant (Fig. 3*A*), no extended density is observed at the potential +1 to +7 subsites. Subsite assignment was determined from structural alignment of CrISA-M7 with the structure of Trex in complex with acarbose (PDB code 2VNC). Overall, there is substantial hydrogen bonding of the M7 to the side chains of residues Glu-640, Arg-450, Asp-620, His-619, Asn-704, Tyr-314, Tyr-706, Arg-389, Trp-229, Thr-228 and the main chain of residues Tyr-331, Gly-417, Asn-387, and Tyr-315. A schematic representation of the CrISA1-M7 interactions is shown in Fig. 4. Moreover, from *B*-factor analysis and hydrogen bonding interactions with M7, it appears that the majority of the stabilizing interactions occur with the G1, G2, and G3 glucosyl moieties (Fig. 5).

The M7 binds to the active site cleft in an "S" shaped configuration and with a distinct kink occurring between the G3 and G4 glucosidic bond (Fig. 5). In this configuration, the O6 groups of G7, G6, G5, and G4 glucosyl moieties are in *syn* with one another, and likewise are the O6 groups of the G3, G2, and G1 moieties, whereas the two sections are *anti* to one another. The ϕ (O5-C1-O4-C4) and φ (C1-O4-C4-C3) torsion angles of the G3-G4 glucosidic bond are 38.0° and 83.8°, respectively, and differ from the ϕ and φ angles of the *syn* attached glucoses, which range from 88.7 to 129.3° and 83.8 to 129°, respectively.

Except for G1, the conformations of the individual glucosyl groups are in the energetically favored chair configuration. As covalently linked to Asp-452, the G1 sugar is distorted toward a half-chair conformation, exhibiting a C2-C1-O5-C5 torsion angle of −12° (Fig. 3*B*). This configuration is stabilized through interactions between CO6 and OD2 of Asp-542, CO3 and CO_2 with D620, and π-stacking interaction with Tyr-331 (Figs. 3*B* and 4).

To determine whether there is an active site conformation change that occurs during the binding of M7, we compared the CrISA structure with and without bound M7. Only monomer A was used for the structural analysis of the active site, as the

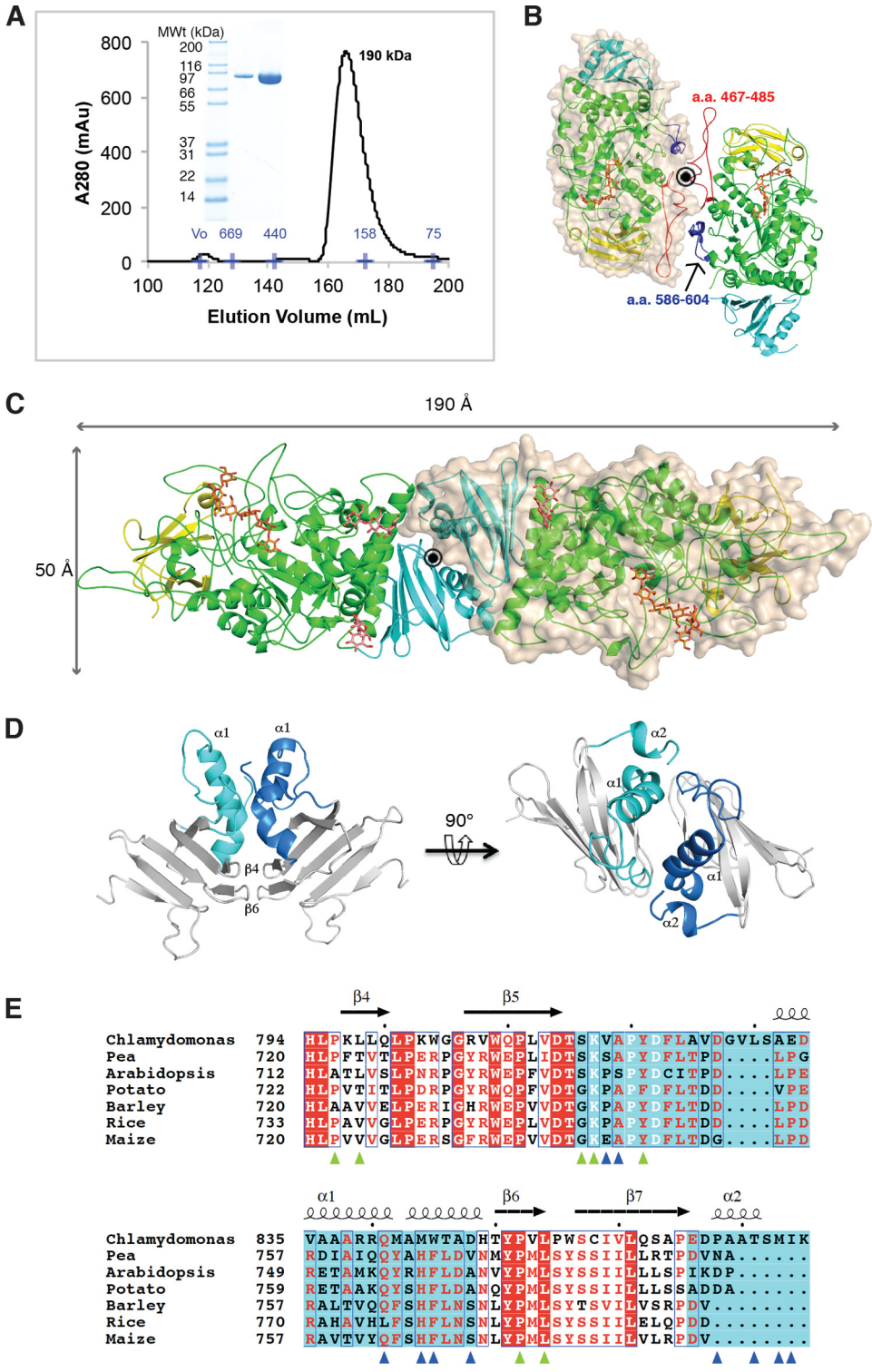

FIGURE 2. **Structure of the CrISA dimer and interface.** *A,* size exclusion chromatography and SDS-PAGE gel (*inset*) of purified CrISA1. Void (V_o) and elution volumes of molecular mass (in kDa) standards are labeled in *blue*. *B*, arrangement of two CrISA1 monomers in the asymmetric unit of the crystal. The N, A, and C subdomains of each monomer are colored *yellow*, *green*, and *cyan*, respectively. Insertional loops (aa 467–485 and 586–604) involved in the crystallographic interface, are colored *red* and *blue*, respectively. ⊙ indicates a 2-fold axis relating the CrISA1 monomers. *C,* biological assembly of the CrISA1 dimer as determined by PISA analysis. Approximate dimensions are displayed Å. Maltoheptaose molecules bound in the active sites are represented in *orange sticks* and maltotriosyl residues in the surface binding sites as *pink sticks*. Coloring of the subdomains is described in *B. D,* zoomed-in views of the C-terminal dimer interface. Colored in *cyan* and *blue* are the loop helix α1 and helix α2 elements of the dimerization interface. The β-strands participating in the interface are labeled β4 and β6. *E*, multiple sequence alignment of the C-terminal region of *Chlamydomonas* (AAP88032), pea (AAZ81835), *Arabidopsis* (AEC09752), potato (AAN15317), barley (AAM46866), rice (ACY56095), and maize (ACG43008). Highlighted in *cyan* is the loop-helix motifs and helix α2 involved in dimerization. Hydrogen-bonding and non-hydrogen bonding interface residues of CrISA1 are indicated in *blue* and *green triangles*, respectively. Alignment was generated using ClustalW (50) and prepared using Espript (51).

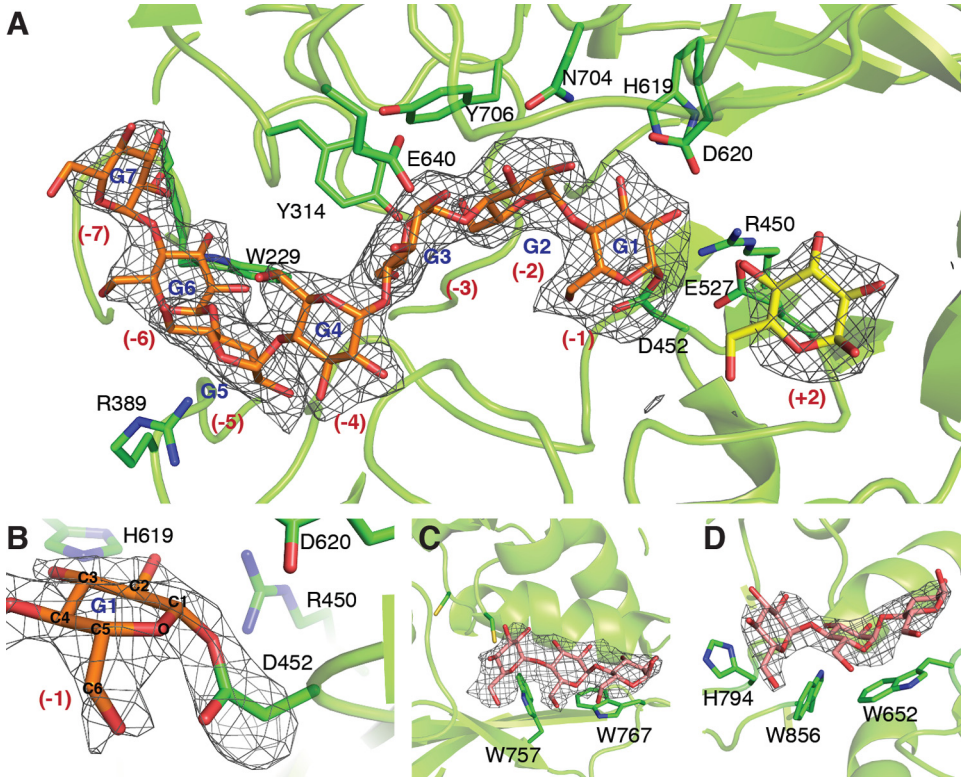

FIGURE 3. **Active site and secondary binding sites in CrISA1.** *A*, substrate binding cleft of CrISA1 (monomer A) with bound maltoheptaose (*orange*) and glucose molecule (*yellow*). Selected substrate binding residues are displayed as *green sticks*. Glucosyl moieties of M7 are labeled G1 to G7 in *blue* and putative substrate binding subsites are labeled in *red*. *B*, zoom-in of the CrISA1 active site displaying the covalent bond between the G1 moiety of maltoheptaose and Asp-452. The contour map displayed in *A* and *B* is the $F_o - F_c$ omit map, with maltoheptaose and the Asp-452 side chain omitted from map calculation, contoured at 3.0 σ and 5.0 σ, respectively. *C*, SBS1, and *D*, SBS2 carbohydrate binding sites. $F_o - F_c$ omit maps surrounding the maltotriose moieties (*pink*) are contoured at 3.0 σ.

active site of monomer B was partly occluded by crystallographic related molecules. Overlaying the structures reveals that in monomer A, there is a narrowing of the groove upon binding of substrate. In particular, loop 629–652 moves up to 3 Å closer toward the bound M7 (Fig. 5). The movement allows hydrogen bonding to occur between Glu-640 and the O2 group of G3, Asn-704 with the O2 and O4 groups of G2, and Tyr-314 with the O6 group of G3. There is also a substantial conformation change in the catalytic residue Asp-620, allowing for hydrogen bonding interaction with the O3 group of G1 (Fig. 5). Although, no other structural movements outside the active site were observed, we cannot discount the possibility that given our post-soaking conditions, that these rearrangement may be constrained due to crystal packing.

Carbohydrate Surface Binding Site—In addition to fitting the M7 oligosaccharide in the active site of CrISA1, we were able to build maltotriose into electron densities located on two distinct surface sites in each monomer (Fig. 3, *C* and *D*). We identified these regions as secondary binding sites (SBS); non-catalytic carbohydrate binding sites found on the surface of the catalytic domain that interact with sugar rings via stacking interactions with aromatic residues (44). These sites, termed SBS1 and SBS2, are located at the reducing end of the active site cleft and at the interface of the catalytic and C-terminal domains, respectively (Fig. 2*B*). Although we have been able to model maltotriose residues in the electron density, it is likely these glucosyl residues represent only the ordered portion of the M7 oligosaccharide, which had been soaked into the crystal. In both sites, the maltotriose oligosaccharide binds with a slight curvature, hinting at the possibility that these sites might recognize the helical structure of crystalline amylopectin. At the SBS1 site, the maltotriose interacts via stacking interactions with aromatic residues, Trp-757 and Trp-767 (Fig. 3*A*), and in the SBS2 site, stacking interactions occurs through residues Trp-652, His-794, and Trp-856 (Fig. 3*B*). *B*-factor analysis of the bound maltotriose suggests that the interaction is more stable in the SBS1 site compared with SBS2. Additionally, the weak electron density in the SBS2 site of monomer B did not allow proper fitting of glycosyl residues, most likely due to its proximity to a crystal-packing interface.

Functional Complementation of sta8 Mutants with Wild-type ISA2 and ISA2-HA—The structure of the CrISA1 dimer reported above is the first three-dimensional description of the enzyme thought to be responsible for amylopectin crystallization. We subsequently wanted to confirm the nature of the larger oligomeric assemblies in which ISA1 participates *in vivo* (17). As the *Chlamydomonas sta8* mutants display similar starch characteristic to the *isa2* mutants of certain plant species, we wanted to clarify the relationship of the *STA8* locus to the ISA2 protein. We therefore amplified distinct 5′ and 3′ regions from wild-type and mutant *sta8-1*::*ARG7* (strain BAFV13) or *sta8-2*::*ARG7* (strain BAFO6) with primers taken from the N-terminal and C-terminal parts of the *ISA2* gene. Unlike with the wild-type gene, we were unable to amplify frag-

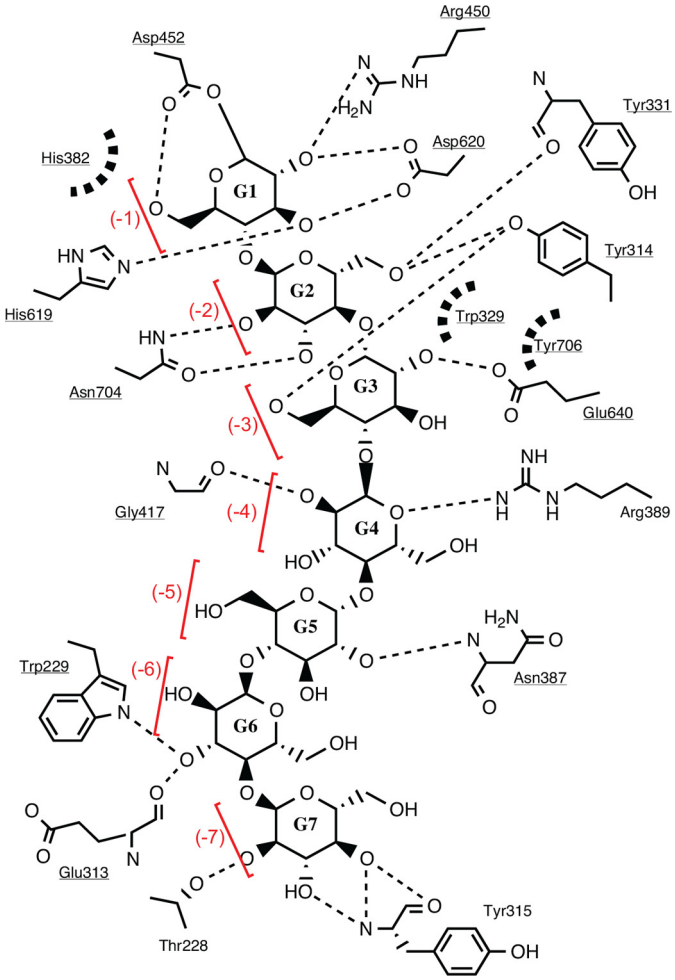

FIGURE 4. **Schematic representation of interaction between CrISA1 active site residues and maltoheptaose.** Shown as *dashed lines* are hydrogen bonding interactions (between 2.8 and 3.2 Å). Dashed half-moons represent hydrophobic interactions. Individual glucosyl rings are labeled G1–G7 from reducing to non-reducing end and substrate-binding subsites are labeled in *red*. The *solid line* between Asp-452 and G1 represents a covalent bond (1.48 Å). *Underlined* residues are absolutely conserved with plant ISA1 (maize, rice, barley, *Arabidopsis*, and potato).

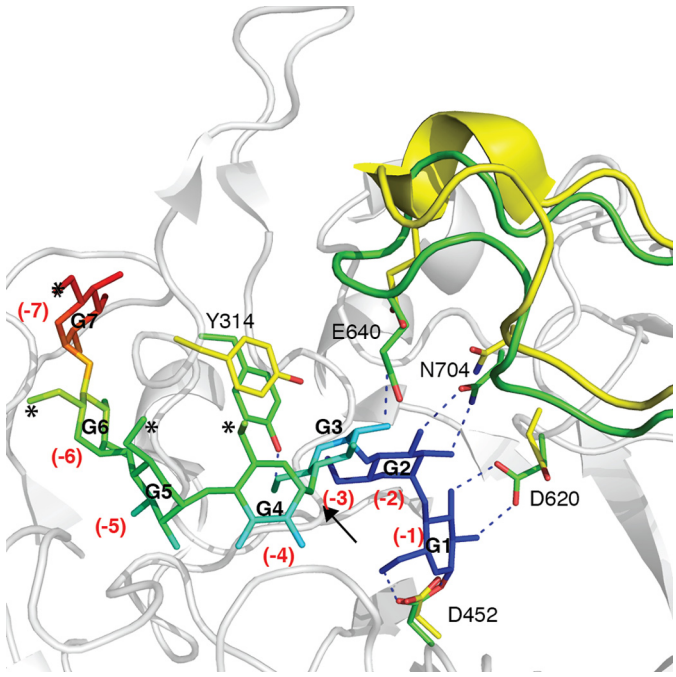

FIGURE 5. **Active site changes in CrISA1 upon binding of maltoheptaose.** Structural differences between the CrISA1 and CrISA1·M7 structures are highlighted in *yellow* and *green*, respectively. These include the loop 629–652, and residues Tyr-314, Asp-620, Glu-640, and Asn-704, which in the CrISA1·M7 structure move closer to the active site to hydrogen bond (*blue dashes*) with the bound M7 ligand. M7, colored according to *B*-factor values (*blue* = lowest and *red* = highest B factor values), binds in an S shape configuration. *Asterisks* mark the solvent-exposed CO6 groups and the *arrow* denotes the location of the kink in the M7 strand. Individual glucosyl rings are labeled G1–G7 and substrate-binding subsites are labeled in *red*.

ments from the 5′ and 3′ regions from all *sta8-1*::*ARG7* carrying strains, whereas only fragments corresponding to the C-terminal could be purified from the *sta8-2*::*ARG7* carrying strains (data not shown). These defects co-segregated in crosses with the corresponding mutant alleles. The two distinct gene disruptions of the *STA8* locus were then complemented with constructs encoding either the wild-type *ISA2* gene or *ISA2* carrying a triple HA tag (*ISA2-HA*). Characteristics of the starch isolated from wild-type strain (330), *sta8* mutant strains (BaFO6 and BaFV13), *sta8*::*ISA2* (O6C and V13C), and *sta8*::*ISA2-HA* (O6HA and V13HA) complemented strains are summarized in Table 1. Under nitrogen starvation, compared with the wild-type 330 strain, mutations in *STA8* yield a 60–80% decrease in starch content, a strong increase in the amylose content, and substantial increase in water-soluble polysaccharide accompanied by a modification of the amylopectin structure. These defects could be reversed when complemented by wild-type *ISA2* in both mutant backgrounds, as exhibited by the O6C and V13C strains, and by wild-type *ISA2-HA*-tagged constructs as exhibited in the O6HA and V13HA strains. These results suggest that *STA8* encodes for ISA2 and that all phenotypic defects previously recorded (15) can be traced to the absence of the ISA2 protein.

In Vivo Interaction of ISA1 and ISA2—We investigated the possible ISA1·ISA2 complex assembly in *Chlamydomonas in vivo*. First, we confirmed the presence of the active ISA1 enzyme in all strains. On a denaturing starch zymogram, extracts of wild-type, *sta8*, BafV13, and V13C and V13HA complemented strains display the 88-kDa band associated with the debranching enzyme activity of ISA1 (19) (Fig. 6*A*). ISA1 complex assemblies were then analyzed on a native glycogen zymogram. We demonstrated that the 3–4 band pattern of varying mobility observed in wild-type is simplified to one fast moving enzyme band in the BafV13 mutant extract (Ref. 17 and Fig. 6*B*). By complementation with *ISA2* and *ISA2-HA* constructs, these features were reverted back to wild-type (Fig. 6*B*). These zymograms demonstrate that ISA2 exists in higher order oligomeric assemblies with ISA1, and that the ISA1 enzyme is also partially functional without ISA2.

We further confirmed the ISA1·ISA2 complex by pulldown assays. ISA2-HA was pulled down from O6HA crude extracts and was run on denaturing starch-containing zymograms. A clear blue band was detected on the HA pulldown lane on the starch containing gel (Fig. 6*C*). From its relative migration to the bands detected in the crude extract, the band was determined to be ISA1 (7). Moreover, no other starch modifying activity (starch synthase and phosphorylase) was detected to

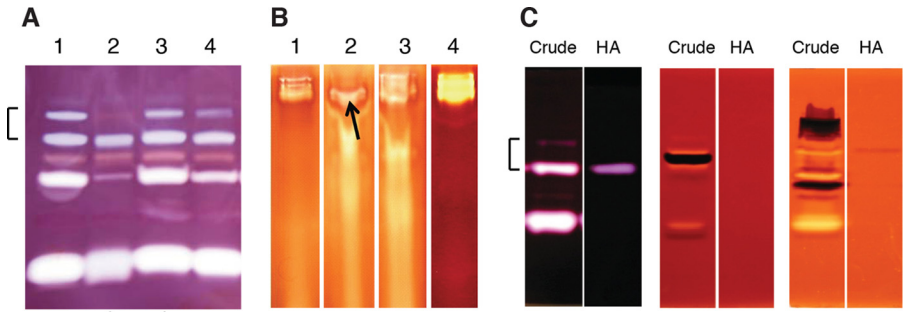

FIGURE 6. **Zymogram detection of starch modifying activities from *Chlamydomonas* extracts.** *A*, detection of debranching activity in denaturing starch zymogram and *B*, native glycogen zymogram in crude extracts from wild-type parental 330 strain (*lane 1*), *sta8* BafV13 mutant strain (*lane 2*), and two complemented strains V13C (*lane 3*) and V13HA (*lane 4*). *C*, detection of starch debranching (*left panel*), phosphorylase (*middle panel*), and starch synthase (*right panel*) activities in O6HA crude and HA pulldown extracts. In the denaturing starch zymograms (*A* and *C*, *left panel*), the *brackets* indicate the two bands associated with ISA1 activity, the lower being the 88-kDa ISA1 protein and the higher being a covalent modification of ISA1 sometimes observed depending on extract preparation. In the native glycogen containing gel B, the *top bands* are associated with activity from ISA1 and ISA1·ISA2 complexes. The *arrow* indicates the ISA1 homomeric complex. In the detection of starch synthase activity (*C*, *right panel*), although the denaturing glycogen zymogram conditions are not optimal for ISA1 activity detection, trace activity can be also seen as a faint brownish band in the HA pull-down lane.

co-elute with ISA2-HA when run on glycogen containing zymograms (Fig. 6*C*).

DISCUSSION

In previous studies, defects in the *STA8* locus were reported to alter starch characteristics and lead to a simplification of the isoamylase zymogram pattern on activity gels (17, 19). There was also at least a 2-fold decrease in apparent size of the isoamylase complex possibly from a hexamer or tetramer to that of a dimer (17). Although these observations have been previously observed in *ISA2* knockdown and mutant studies in maize and rice (11, 14), the molecular nature of the *STA8* locus and its relationship to the *ISA2* gene was lacking from the initial studies in *Chlamydomonas* (17, 19). We now show that starch defects in the *sta8* mutants can be almost fully reversed through functional complementation with wild-type *ISA2* and *ISA2-HA* (Table 1) suggesting the *STA8* locus encodes for *ISA2*.

In our ISA2-HA pulldown assays, we also show that ISA2 interacts with ISA1 (Fig. 6*C*). Combining these results with the previous *STA8* mutant studies and the above mentioned complementation studies, we can now confirm that the ISA1 activity is present in 3 complexes: one ISA1 homomeric and two larger ISA1·ISA2 heteromeric complexes, similar to that observed in the maize and rice species (10, 11). In the wild-type strain, all three complexes exist and range in size from 150 to 500 kDa (as determined by gel permeation chromatography, GPC) (45), whereas in *sta8* mutants, the two larger complexes disappear leaving an ISA1 homodimer at a size of 150 kDa (17). We have also demonstrated that the recombinant CrISA1 exists as a stable dimer (Fig. 2, *A* and *C*).

The fact that mutants lacking ISA2 are still able both to assemble a functional isoamylase and to sustain normal rates of starch synthesis in nitrogen-supplied medium, and decreased but significant rates of semi-crystalline starch synthesis under nitrogen starvation (19), suggests that the dimeric structure of ISA1 described in detail in this work is able to sustain starch synthesis *in vivo*, at least in alga. Through structural analysis as describe below, we investigated possible features in the ISA1 dimer that would allow it to accomplish its role in branch trimming.

We have determined the crystal structure of CrISA1 to 2.3 Å and CrISA1·M7 to 2.4 Å. The overall structure reveals an elongated shape formed by the dimerization of two monomers in a tail-to-tail manner via their C termini (Fig. 2*C*). Moreover, through crystal complex studies with maltoheptaose (M7), we have mapped the active site, branch recognition cleft, and additional SBS (Fig. 3, *A*, *C*, and *D*). The covalent bond between M7 and the catalytic nucleophile D452 (Fig. 3*B*) suggests formation of a glycosyl-enzyme intermediate; a characteristic intermediary state in the two-step reaction mechanism of retaining glycosyl hydrolases. It has been notoriously difficult to trap substrates in wild-type family 13 glycoside hydrolase enzymes due to the high catalytic turnover rates and/or transglycosylating activities. Other intermediate trapping studies in family 13 glycoside hydrolase enzymes have been investigated with cyclodextrin transferase and human pancreatic α-amylase, however, these studies involved modified substrates and/or mutant enzymes (46, 47). Our approach was to soak in high concentrations of M7, a hydrolysis product, to trap an intermediate through the reverse mechanism. As ISA1 is not known to possess transglycosylating activities, and likewise does not have a defined (+) acceptor-binding site (Fig. 3*A*), the M7 was fortuitously trapped in the CrISA1 active site. The CrISA1·M7 complex can be considered a trapped intermediate of a released branch product, and structural analysis into the binding of the "branch" provides insights into the substrate specificity of CrISA1.

We have shown from activity assays that the recombinant CrISA1 displays similar activity to that of the purified plant ISA1 in its substrate preference for long branches of AP, β-limit dextrin and glycogen, and low activity toward pullulan (Fig. 1*A*). As witnessed from the binding of maltoheptaose in the CrISA1 structure, M7 binds in a twisted "S" structure (Fig. 5). In this configuration the CO6 groups from the G1, G2, and G3 moieties are either buried or hydrogen bonded to the active site residues, whereas those of G4, G5, G6, and G7 are solvent exposed (Figs. 4 and 5). This suggests that the mechanism for branch recognition requires the CO6 group of the G1, G2, and G3 adjacent to the α1,6-branch to be accessible for optimal interaction with the CrISA1 active site. These observations

explain the low activity of CrISA1 in hydrolyzing the α1,6-linked maltotriose motifs observed in pullulan. If pullulan were to reside in the substrate-binding site, the branched glucosyl group would be positioned in the +1 and additionally the −3 subsites. Due to steric hindrance, it is unlikely that the branched glucosyl residue in the −3 subsite could bind in a conformation that would allow for Tyr-314 and Glu-640 hydrogen bonding interactions, as observed with the G3 glucosyl group of a linear M7 molecule (Figs. 4 and 5). Thus binding affinity would likely be reduced in pullulan compared with substrates with branches spaced further apart. In terms of the role of CrISA1 in branch trimming, we would predict that the enzyme would be less efficient at targeting densely spaced branches separated by less than 4 glucosyl units. Moreover, as the substrate-binding groove of CrISA1 only accommodates a single oligosaccharide chain, in physiological substrates, the enzyme is likely to pass over branches that are involved in double helical strands and hydrolyze more accessible single-chained branches.

The CrISA1 sequence shares ~51–54% sequence identity and 63–65% similarity to those of plant ISA1 and thus can potentially serve as a good model for better understanding the plant enzymes. Sequence alignment of selected plant ISA1 with CrISA1 reveals high conservation in the catalytic core (Fig. 7). Closer examination of the alignment reveals that active site residues are absolutely conserved and substrate-binding residues are conserved from subsites −6 to −1 (Figs. 4 and 7). This suggests that the mechanism of branch recognition and mechanism for hydrolysis is highly conserved in ISA1.

CrISA1 has three additional loops (aa 216–226, 467–485, and 585–603) that are not present in the plant ISA1 sequences (Figs. 7 and 8A). It should be noted that in the crystal asymmetric unit, loops 467–485 and 585–603 interact with one another to form a buried interface area of 785 Å^2, representing 2.6% of the total monomer surface area (Fig. 2*B*). This interface is unlikely to exist stably in the solution, as our gel filtration experiments of CrISA1 do not reveal significant amounts of tetrameric or higher order oligomeric species (Fig. 2*a*). However, *in vivo* experiments have shown the existence of the higher oligomeric ISA1/ISA2 species (Fig. 6*B*), but only in the presence of ISA2. We therefore cannot exclude the possibility that the loops contribute toward the formation of interface in higher oligomeric species and that ISA2 is required for in-solution stabilization of this interface.

We also investigated whether the dimeric tail-to-tail arrangement of CrISA1 could be conserved in other plant ISA1. The sequences encoding the structural features of the CrISA1 dimer interface were identified and compared with those of plant ISA1. Sequence alignment reveals that the structural loop-helix inserted between strands β-5 and β-6 is conserved in all ISA1 sequences and so is the hydrophobic character of the interface residues from the β4- and β6-strands (Fig. 2, *D* and *E*). Moderate conservation is observed in interface residues participating in non- and hydrogen bonding interactions, at least among the plant species (Fig. 2*E*). The conservation of several interface elements suggests that it is highly possible that the dimeric arrangement seen in the CrISA1 is maintained in other plant species. Further analysis of the ISA1·ISA2 complex in *Arabidopsis* in the next section shows additional support of this hypothesis.

Sundberg *et al.* (48) investigated the structural assembly of the *Arabidopsis* ISA1·ISA2 heteromer isolated by tandem-affinity purification. Transmission electron microscopy visualization of the ISA1·ISA2 complex revealed an elongated dumbbell structure composed of two lobes (48). We revisited the idea that the ISA1 interface is conserved in plant ISA1, as the elongated shape of the *Arabidopsis* ISA1·ISA2 complex is reminiscent of the shape of the CrISA1 homodimer structure, although the ISA1·ISA2 structures have more prominent lobes. As the *Arabidopsis* ISA1·ISA2 complex was estimated to be ~30 nm in length and that of the CrISA1 dimer was shown to be ~19 nm (190 Å) (Fig. 2*C*), we propose that assembly of the ISA1·ISA2 heteromer is based on an ISA1 dimer scaffold (linked end-to-end as described by the CrISA1 crystal structure), with two additional ISA2 modules overlapping with ISA1 in their N-terminal regions, creating the prominent lobes. Without a higher resolution ISA1·ISA2 complex structure, we cannot predict exactly where and how ISA2 would bind. As ISA1 has been shown to exist without ISA2, at least in cereals and *Chlamydomonas*, whereas in *Arabidopsis* and potato, both ISA1 and ISA2 subunits are required for heteromer formation, the ISA1/ISA2 interface is unlikely to be conserved throughout all plants species but more likely to be conserved among the plant species that display similar ISA1·ISA2 complex distributions. Interestingly, the N-terminal region of ISA1, which is found to be disordered in the CrISA1 structure (residues 57–77), is conserved within monocots and dicots (49). The N-terminal regions of ISA1 may thus serve to mediate ISA1-ISA2 interactions.

One outstanding question that remains to be answered is how the ISA1·ISA2 complex facilitates crystallization of starch. By solving the first structure of the ISA1 dimer from *Chlamydomonas* in complex with M7, we are closer toward understanding the mechanism by which the enzyme trims misplaced amylopectin branches. Although the exact physiological substrate of ISA1 remains to be determined, the CrISA1 structure in complex with M7 reveals the molecular details of how ISA1 recognizes single-stranded branches and why tightly spaced branches are unfavorable targets for the enzyme. Moreover, the structure reveals additional SBS features and several loops that are unique to CrISA1 (Fig. 8*A*). Although we do not yet know the exact roles of the SBS1 and SBS2 there are numerous roles reportedly associated with SBS, including the recognition of starch structures, substrate targeting, and substrate guidance into the active site (44). Moreover, it is interesting to note the arrangement of the two substrate-binding grooves in relationship to one another. In the dimeric arrangement, the binding groove of each monomer is placed in such a way that in terms of their non-reducing ends, the branches from the target substrate (Fig. 8*B*) are binding in opposition to one another (Fig. 8*A*). Whether the active sites work together on the same target substrate to enable proper trimming of amylopectin has not been studied. Until we have a better understanding of structural features of the physiological substrate of CrISA1, we can only speculate about the cooperativity between the active sites of the two monomers. That is, perhaps assembly of the ISA1 dimer provides an ideal platform with multiple interaction points, which

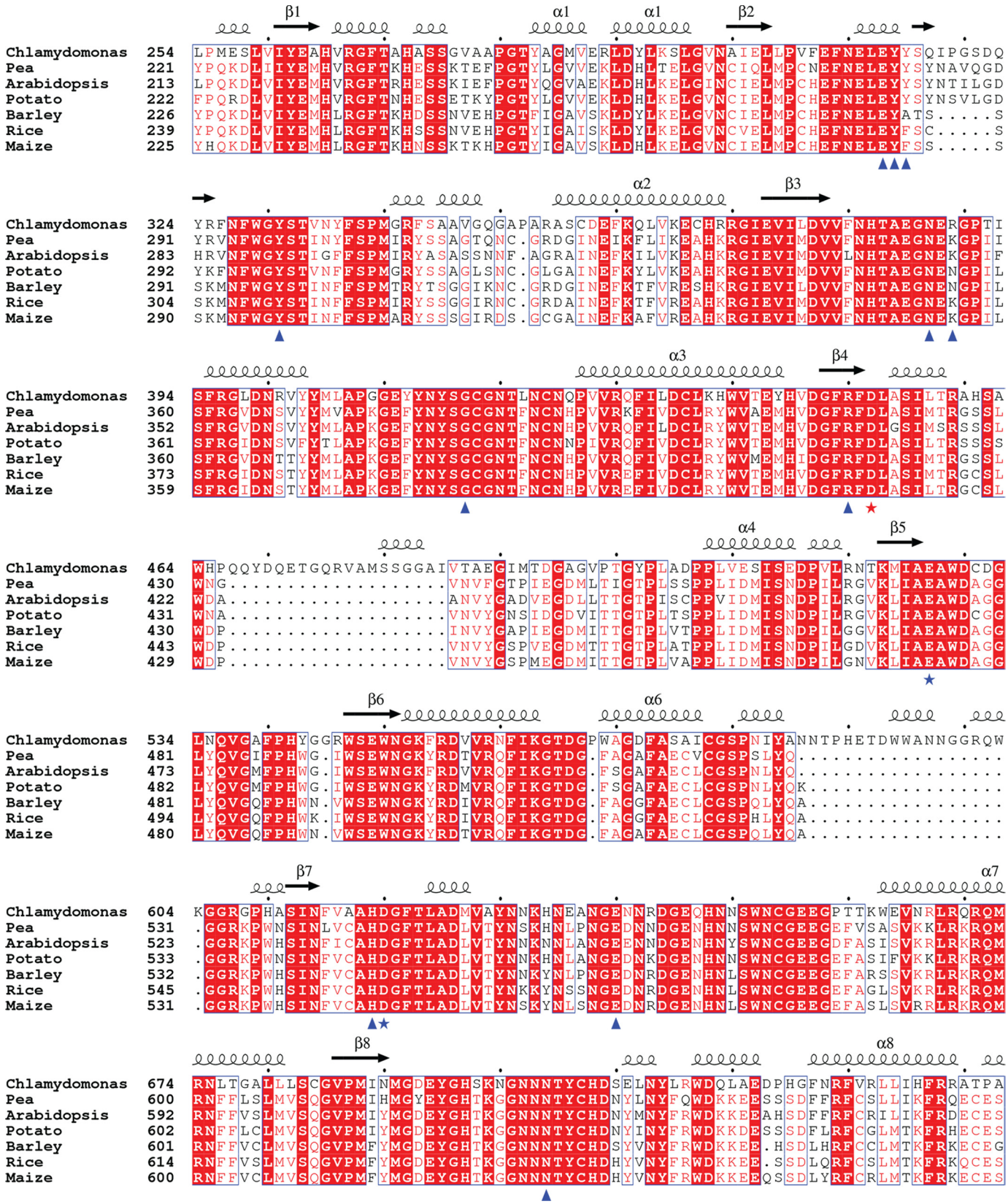

FIGURE 7. **Multiple sequence alignment of plant ISA1.** Shown is the alignment of the catalytic subdomain of ISA1 from *Chlamydomonas* and representative plant species. Alignment and sequences are described in the legend to Fig. 2*C*. Secondary structural elements shown *above* the alignment correspond to the CrISA1 structure. *Stars* mark catalytic triad residues of CrISA with the nucleophile in *red* and acid/base residues in *blue*. Hydrogen bonding residues to the maltoheptaose are marked with *blue triangles*. Alignment was generated using ClustalW (50) and prepared using Espript (51).

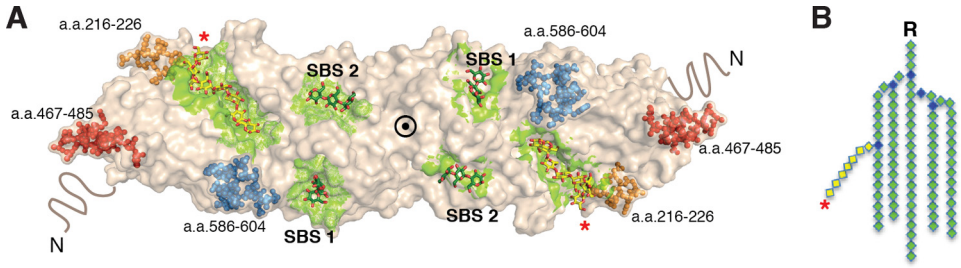

FIGURE 8. **Structural features of the CrISA1 dimer.** *A*, shown is the dimeric structure of CrISA1 highlighting the arrangement of carbohydrate binding sites (*green*) and three loop regions unique to CrISA1 (*orange*, *red*, and *blue spheres*). At the N-terminal regions indicated by *N*, disordered residues (aa 57–77) are drawn as *wavy lines*. *B*, schematic representation of a portion of an amylopectin cluster. *Green diamonds* represent linear α1,4-linked glucosyl units, whereas the *blue diamonds* represent the α1,6-linked glucosyl branch points. For molecule orientation in *A* and *B*, the reducing end of the branched saccharide is indicated by an *R* and non-reducing end of the branch portion to be cleaved is indicated by the *asterisk*.

could coordinate with one another to determine the specific branching pattern required for proper amylopectin processing and crystallization. These SBS sites and possible ISA1/ISA2 interfaces would merit further investigation through *in vitro* and *in vivo* mutational work not only in *Chlamydomonas*, but also in other plant ISA1·ISA2 starch debranching complexes.

Acknowledgments—We acknowledge the European Synchrotron Radiation Facility and beamline scientists at ID23-1 and ID23-2 for beam time and assistance, Dr. Jose Antonio Cuesta-Seijo for collecting diffraction data and assisting in the data processing of the CrISA1·M7 crystal, Dr. Alexander Striebeck for assistance with the enzymology, and we thank DANSCATT for access to synchrotron beam time.

REFERENCES

1. Buléon, A., Colonna, P., Planchot, V., and Ball, S. (1998) Starch granules: structure and biosynthesis. *Int. J. Biol. Macromol.* **23,** 85–112
2. Zeeman, S. C., Kossmann, J., and Smith, A. M. (2010) Starch: its metabolism, evolution, and biotechnological modification in plants. *Annu. Rev. Plant. Biol.* **61,** 209–234
3. Pérez, S., and Bertoft, E. (2010) The molecular structures of starch components and their contribution to the architecture of starch granules: a comprehensive review. *Starch/Stärke* **62,** 389–420
4. Nakamura, Y. (2002) Towards a better understanding of the metabolic system for amylopectin biosynthesis in plants: rice endosperm as a model tissue. *Plant Cell Physiol.* **43,** 718–725
5. Ball, S. G., and Morell, M. K. (2003) From bacterial glycogen to starch: understanding the biogenesis of the plant starch granule. *Annu. Rev. Plant Biol.* **54,** 207–233
6. Zeeman, S. C., Umemoto, T., Lue, W. L., Au-Yeung, P., Martin, C., Smith, A. M., and Chen, J. (1998) A mutant of Arabidopsis lacking a chloroplastic isoamylase accumulates both starch and phytoglycogen. *Plant Cell* **10,** 1699–1712
7. Mouille, G., Maddelein, M. L., Libessart, N., Talaga, P., Decq, A., Delrue, B., and Ball, S. (1996) Preamylopectin processing: a mandatory step for starch biosynthesis in plants. *Plant Cell* **8,** 1353–1366
8. James, M. G., Robertson, D. S., and Myers, A. M. (1995) Characterization of the maize gene sugary1, a determinant of starch composition in kernels. *Plant Cell* **7,** 417–429
9. Myers, A. M., Morell, M. K., James, M. G., and Ball, S. G. (2000) Recent progress toward understanding biosynthesis of the amylopectin crystal. *Plant Physiol.* **122,** 989–997
10. Utsumi, Y., and Nakamura, Y. (2006) Structural and enzymatic characterization of the isoamylase1 homo-oligomer and the isoamylase1-isoamylase2 hetero-oligomer from rice endosperm. *Planta* **225,** 75–87
11. Kubo, A., Colleoni, C., Dinges, J. R., Lin, Q., Lappe, R. R., Rivenbark, J. G., Meyer, A. J., Ball, S. G., James, M. G., Hennen-Bierwagen, T. A., and Myers, A. M. (2010) Functions of heteromeric and homomeric isoamylase-type starch-debranching enzymes in developing maize endosperm. *Plant Physiol.* **153,** 956–969
12. Bustos, R., Fahy, B., Hylton, C. M., Seale, R., Nebane, N. M., Edwards, A., Martin, C., and Smith, A. M. (2004) Starch granule initiation is controlled by a heteromultimeric isoamylase in potato tubers. *Proc. Natl. Acad. Sci. U.S.A.* **101,** 2215–2220
13. Delatte, T., Trevisan, M., Parker, M. L., and Zeeman, S. C. (2005) Arabidopsis mutants Atisa1 and Atisa2 have identical phenotypes and lack the same multimeric isoamylase, which influences the branch point distribution of amylopectin during starch synthesis. *Plant J.* **41,** 815–830
14. Utsumi, Y., Utsumi, C., Sawada, T., Fujita, N., and Nakamura, Y. (2011) Functional diversity of isoamylase oligomers: the ISA1 homo-oligomer is essential for amylopectin biosynthesis in rice endosperm. *Plant Physiol.* **156,** 61–77
15. Buléon, A., Gallant, D. J., Bouchet, B., Mouille, G., D'Hulst, C., Kossmann, J., and Ball, S. (1997) Starches from A to C: *Chlamydomonas reinhardtii* as a model microbial system to investigate the biosynthesis of the plant amylopectin crystal. *Plant Physiol.* **115,** 949–957
16. Libessart, N., Maddelein, M. L., Koornhuyse, N., Decq, A., Delrue, B., Mouille, G., D'Hulst, C., and Ball, S. (1995) Storage, photosynthesis, and growth: the conditional nature of mutations affecting starch synthesis and structure in *Chlamydomonas*. *Plant Cell* **7,** 1117–1127
17. Dauvillée, D., Colleoni, C., Mouille, G., Morell, M. K., d'Hulst, C., Wattebled, F., Liénard, L., Delvallé, D., Ral, J. P., Myers, A. M., and Ball, S. G. (2001) Biochemical characterization of wild-type and mutant isoamylases of *Chlamydomonas reinhardtii* supports a function of the multimeric enzyme organization in amylopectin maturation. *Plant Physiol.* **125,** 1723–1731
18. Work, V. H., Radakovits, R., Jinkerson, R. E., Meuser, J. E., Elliott, L. G., Vinyard, D. J., Laurens, L. M., Dismukes, G. C., and Posewitz, M. C. (2010) Increased lipid accumulation in the *Chlamydomonas reinhardtii* sta7–10 starchless isoamylase mutant and increased carbohydrate synthesis in complemented strains. *Eukaryotic Cell* **9,** 1251–1261
19. Dauvillée, D., Colleoni, C., Mouille, G., Buléon, A., Gallant, D. J., Bouchet, B., Morell, M. K., d'Hulst, C., Myers, A. M., and Ball, S. G. (2001) Two loci control phytoglycogen production in the monocellular green alga *Chlamydomonas reinhardtii*. *Plant Physiol.* **125,** 1710–1722
20. Harris, E. H. (1989) *The Chlamydomonas sourcebook. A Comprehensive Guide to Biology and Laboratory Use.* Academic Press, San Diego
21. Dauvillée, D., Chochois, V., Steup, M., Haebel, S., Eckermann, N., Ritte, G., Ral, J.-P., Colleoni, C., Hicks, G., Wattebled, F., Deschamps, P., d'Hulst, C., Liénard, L., Cournac, L., Putaux, J.-L., Dupeyre, D., and Ball, S. G. (2006) Plastidial phosphorylase is required for normal starch synthesis in *Chlamydomonas reinhardtii*. *Plant J.* **48,** 274–285
22. Kindle, K. L. (1990) High-frequency nuclear transformation of *Chlamydomonas reinhardtii*. *Proc. Natl. Acad. Sci. U.S.A.* **87,** 1228–1232
23. Delrue, B., Fontaine, T., Routier, F., Decq, A., Wieruszeski, J. M., Van Den Koornhuyse, N., Maddelein, M. L., Fournet, B., and Ball, S. (1992) Waxy *Chlamydomonas reinhardtii*: monocellular algal mutants defective in amylose biosynthesis and granule-bound starch synthase activity accumulate a structurally modified amylopectin. *J. Bacteriol.* **174,** 3612–3620
24. Emanuelsson, O., Nielsen, H., and von Heijne, G. (1999) ChloroP, a neural network-based method for predicting chloroplast transit peptides and

their cleavage sites. *Protein Sci.* **8,** 978–984
25. Kabsch, W. (2010) *XDS*. *Acta Crystallogr. D Biol. Crystallogr.* **66,** 125–132
26. Weiss, M. S. (2001) Global indicators of x-ray data quality. *J. Appl. Crystallogr.* **34,** 130–135
27. Evans, P. R., and Murshudov, G. N. (2013) How good are my data and what is the resolution? *Acta Crystallogr. D Biol. Crystallogr.* **69,** 1204–1214
28. Karplus, P. A., and Diederichs, K. (2012) Linking crystallographic model and data quality. *Science* **336,** 1030–1033
29. McCoy, A. J., Grosse-Kunstleve, R. W., Adams, P. D., Winn, M. D., Storoni, L. C., and Read, R. J. (2007) Phaser crystallographic software. *J. Appl. Crystallogr.* **40,** 658–674
30. Stein, N. (2008) CHAINSAW: a program for mutating pdb files used as templates in molecular replacement. *J. Appl. Crystallogr.* **41,** 641–643
31. Woo, E.-J., Lee, S., Cha, H., Park, J.-T., Yoon, S.-M., Song, H.-N., and Park, K.-H. (2008) Structural insight into the bifunctional mechanism of the glycogen-debranching enzyme TreX from the archaeon *Sulfolobus solfataricus*. *J. Biol. Chem.* **283,** 28641–28648
32. Langer, G., Cohen, S. X., Lamzin, V. S., and Perrakis, A. (2008) Automated macromolecular model building for x-ray crystallography using ARP/wARP version 7. *Nat. Protoc.* **3,** 1171–1179
33. Emsley, P., Lohkamp, B., Scott, W. G., and Cowtan, K. (2010) Features and development of Coot. *Acta Crystallogr. D Biol. Crystallogr.* **66,** 486–501
34. Winn, M. D., Isupov, M. N., and Murshudov, G. N. (2001) Use of TLS parameters to model anisotropic displacements in macromolecular refinement. *Acta Crystallogr. D Biol. Crystallogr.* **57,** 122–133
35. Murshudov, G. N., Vagin, A. A., and Dodson, E. J. (1997) Refinement of macromolecular structures by the maximum-likelihood method. *Acta Crystallogr. D Biol. Crystallogr.* **53,** 240–255
36. Lebedev, A. A., Young, P., Isupov, M. N., Moroz, O. V., Vagin, A. A., and Murshudov, G. N. (2012) JLigand: a graphical tool for the CCP4 template-restraint library. *Acta Crystallogr. D Biol. Crystallogr.* **68,** 431–440
37. Nelson, N. (1944) A photometric adaptation of the Somoygi method for the determination of glucose. *J. Biol. Chem.* **153,** 375–380
38. Somogyi, M. (1952) Notes on sugar determination. *J. Biol. Chem.* **195,** 19–23
39. Cantarel, B. L., Coutinho, P. M., Rancurel, C., Bernard, T., Lombard, V., and Henrissat, B. (2009) The Carbohydrate-Active EnZymes database (CAZy): an expert resource for glycogenomics. *Nucleic Acids Res.* **37,** D233-D238
40. Katsuya, Y., Mezaki, Y., Kubota, M., and Matsuura, Y. (1998) Three-dimensional structure of *Pseudomonas* isoamylase at 2.2-Å resolution. *J. Mol. Biol.* **281,** 885–897
41. Song, H.-N., Jung, T.-Y., Park, J.-T., Park, B.-C., Myung, P. K., Boos, W., Woo, E.-J., and Park, K.-H. (2010) Structural rationale for the short branched substrate specificity of the glycogen debranching enzyme GlgX. *Proteins* **78,** 1847–1855
42. Krissinel, E., and Henrick, K. (2007) Inference of macromolecular assemblies from crystalline state. *J. Mol. Biol.* **372,** 774–797
43. Davies, G. J., Wilson, K. S., and Henrissat, B. (1997) Nomenclature for sugar-binding subsites in glycosyl hydrolases. *Biochem. J.* **321,** 557–559
44. Cuyvers, S., Dornez, E., Delcour, J. A., and Courtin, C. M. (2012) Occurrence and functional significance of secondary carbohydrate binding sites in glycoside hydrolases. *Crit. Rev. Biotechnol.* **32,** 93–107
45. Dauvillée, D., Mestre, V. V., Colleoni, C., Slomianny, M., Mouille, G., Delrue, B., d'Hulst, C., Bliard, C., Nuzillard, J., and Ball, S. (2000) The debranching enzyme complex missing in glycogen accumulating mutants of *Chlamydomonas reinhardtii* displays an isoamylase-type specificity. *Plant Sci.* **157,** 145–156
46. Uitdehaag, J. C., Mosi, R., Kalk, K. H., van der Veen, B. A., Dijkhuizen, L., Withers, S. G., and Dijkstra, B. W. (1999) X-ray structures along the reaction pathway of cyclodextrin glycosyltransferase elucidate catalysis in the α-amylase family. *Nat. Struct. Biol.* **6,** 432–436
47. Zhang, R., Li, C., Williams, L. K., Rempel, B. P., Brayer, G. D., and Withers, S. G. (2009) Directed "*in situ*" inhibitor elongation as a strategy to structurally characterize the covalent glycosyl-enzyme intermediate of human pancreatic α-amylase. *Biochemistry* **48,** 10752–10764
48. Sundberg, M., Pfister, B., Fulton, D., Bischof, S., Delatte, T., Eicke, S., Stettler, M., Smith, S. M., Streb, S., and Zeeman, S. C. (2013) The heteromultimeric debranching enzyme involved in starch synthesis in *Arabidopsis* requires both isoamylase1 and isoamylase2 subunits for complex stability and activity. *PLoS ONE* **8,** e75223
49. Lin, Q., Facon, M., Putaux, J.-L., Dinges, J. R., Wattebled, F., D'Hulst, C., Hennen-Bierwagen, T. A., and Myers, A. M. (2013) Function of isoamylase-type starch debranching enzymes ISA1 and ISA2 in the *Zea mays* leaf. *New Phytol.* **200,** 1009–1021
50. Larkin, M. A., Blackshields, G., Brown, N. P., Chenna, R., McGettigan, P. A., McWilliam, H., Valentin, F., Wallace, I. M., Wilm, A., Lopez, R., Thompson, J. D., Gibson, T. J., and Higgins, D. G. (2007) Clustal W and Clustal X version 2.0. *Bioinformatics* **23,** 2947–2948
51. Gouet, P., Courcelle, E., Stuart, D. I., and Métoz, F. (1999) ESPript: analysis of multiple sequence alignments in PostScript. *Bioinformatics* **15,** 305–308
52. Chen, V. B., Arendall, W. B., 3rd, Headd, J. J., Keedy, D. A., Immormino, R. M., Kapral, G. J., Murray, L. W., Richardson, J. S., and Richardson, D. C. (2010) MolProbity: all-atom structure validation for macromolecular crystallography. *Acta Crystallogr. D Biol. Crystallogr.* **66,** 12–21